JOURNAL OF GEOPHYSICAL RESEARCH, VOL. 115, A07303, doi:10.1029/2009JA015115, 2010

Variance of transionospheric VLF wave power absorption

X. Tao,[1] J. Bortnik,[1] and M. Friedrich[2]

Received 18 November 2009; revised 25 January 2010; accepted 19 February 2010; published 9 July 2010.

[1] To investigate the effects of *D*-region electron-density variance on wave power absorption, we calculate the power reduction of very low frequency (VLF) waves propagating through the ionosphere with a full wave method using the standard ionospheric model IRI and in situ observational data. We first verify the classic absorption curves of Helliwell's using our full wave code. Then we show that the IRI model gives overall smaller wave absorption compared with Helliwell's. Using *D*-region electron densities measured by rockets during the past 60 years, we demonstrate that the power absorption of VLF waves is subject to large variance, even though Helliwell's absorption curves are within ±1 standard deviation of absorption values calculated from data. Finally, we use a subset of the rocket data that are more representative of the *D* region of middle- and low-latitude VLF wave transmitters and show that the average quiet time wave absorption is smaller than that of Helliwell's by up to 100 dB at 20 kHz and 60 dB at 2 kHz, which would make the model-observation discrepancy shown by previous work even larger. This result suggests that additional processes may be needed to explain the discrepancy.

Citation: Tao, X., J. Bortnik, and M. Friedrich (2010), Variance of transionospheric VLF wave power absorption, *J. Geophys. Res.*, *115*, A07303, doi:10.1029/2009JA015115.

1. Introduction

[2] Very low frequency (VLF) electromagnetic waves generated on the ground (e.g., lightning, VLF transmission) propagate away from their source in the Earth-ionosphere waveguide and impinge on the bottom side ionosphere. A portion of the wave energy can then leak through the ionosphere and out into space, leading to precipitation of energetic electrons [*Abel and Thorne*, 1998a, 1998b; *Inan et al.*, 1984; *Bortnik et al.*, 2006a, 2006b]. When propagating through the ionosphere, VLF waves suffer energy loss through the frequent collisions of electrons with the neutral atmospheric constituents. In order to determine the effect of the waves on the energetic particle population, the wavefield intensities must be specified, which in turn requires knowledge of wave power reduction through the ionosphere [e.g., *Lehtinen and Inan*, 2009]. Most previous models of calculating VLF wave power reduction through the ionosphere use a set of classic absorption curves, first introduced by *Helliwell* [1965] [e.g., *Inan et al.*, 1984; *Abel and Thorne*, 1998a; *Starks et al.*, 2008]. Helliwell used an ensemble averaged ionosphere electron-density model to calculate the absorption of wave power for 2 kHz and 20 kHz waves during daytime and nighttime as a function of latitude [*Helliwell*, 1965]. However, a recent model-observation comparison [*Starks et al.*, 2008] revealed important discrepancies between predicted and observed wave intensities.

[3] *Starks et al.* [2008] used a composite model to calculate propagation of VLF waves from the ground to space and compared their results with several previous models and wavefields measured from several spacecraft. They found that while their composite model gives results consistent with previous models, the calculated VLF fields are generally higher than the observation by about 20 dB at night and at least 10 dB during daytime when away from the magnetic equator. Proposed explanations include enhanced *D*-region absorption and reflection and conversion of wave energy to quasi-electrostatic modes due to small scale structures caused by transmitters [*Lehtinen and Inan*, 2009]. In this work, we use an updated ionospheric model and in situ observations to investigate the effect of the variance of the *D*-region electron density, thus the *D*-region absorption, on VLF wave damping through the ionosphere.

[4] The collisional absorption of wave power depends primarily on the electron density and its associated collision frequency in the *D* region. The *D*-region electron density is subject to large variance due to complicated processes involved in forming this region [*Schunk and Nagy*, 2004]. Additionally, the measurement of the *D*-region electron density is difficult, because the altitude is too high for balloon observations and too low for satellites and the densities are too low to be measured by ionosondes and radars [*Bilitza*, 2001]. The limited volume of data also makes it difficult to build a reliable *D*-region model [*Bilitza and Reinisch*, 2008]. In his calculation, *Helliwell* [1965] used an averaged *D*-region model that did not vary with latitude. However, the actual *D*-region electron density varies with both latitude and season, thus one natural question of using Helliwell's

[1]Department of Atmospheric and Oceanic Sciences, University of California, Los Angeles, California, USA.
[2]Institute of Communication Networks and Satellite Communications, Graz University of Technology, Graz, Austria.

0148-0227/10/2009JA015115

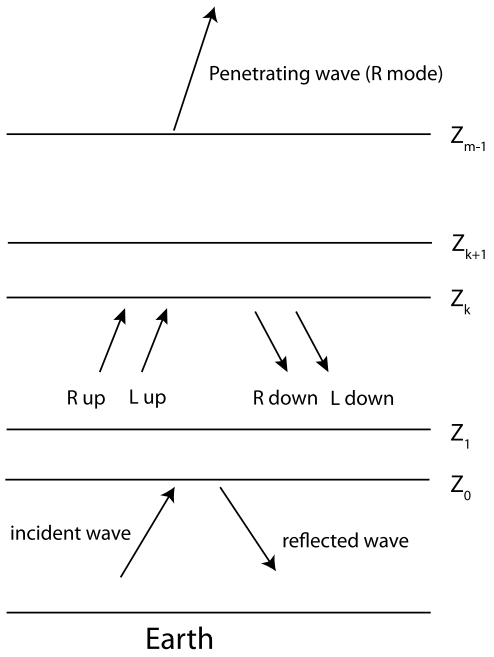

Figure 1. Sketch of the stratified layer model of the ionosphere, with four characteristic wave modes inside a layer shown. The VLF wave that can penetrate through the ionosphere is the R-mode wave.

absorption curves is how they vary due to the variance of the *D*-region electron density. We investigate this problem using a full wave approach, which preserves the full wave effects that are not included in the simple analysis of *Helliwell* [1965], such as energy loss due to internal reflections and conversion to other wave modes.

[5] Our full wave code follows the development of, for example, *Pitteway* [1965] and *Arantes and Scarabucci* [1975] and is described in more detail in Appendix A. The ionosphere is assumed to be a stratified medium as shown in Figure 1, with the *x*-*y* plane parallel to the boundary between layers and the medium is assumed to vary only with height (the *z* direction) [*Budden*, 1985]. Maxwell's equations are then reduced to a set of one-dimensional ordinary differential equations [*Pitteway*, 1965; *Walsh*, 1967; *Lehtinen and Inan*, 2008]. In this work, we use the matrix method proposed by *Nagano et al.* [1975] to solve the reduced Maxwell's equations, because of its efficiency and natural decomposition of total wavefields in the ionosphere to characteristic L-mode and R-mode waves. In the VLF frequency range, it is the upward propagating R-mode wave that can penetrate through the ionosphere into space and whose absorption has been calculated by *Helliwell* [1965]. We solve a generalized full wave equation, briefly described in Appendix A, using the matrix method of *Nagano et al.* [1975].

[6] Using the ionospheric model given by *Helliwell* [1965], we calculate the absorption of VLF waves using our full wave code and compare the results with that of *Helliwell* [1965] in section 2. We then show how the widely used IRI model affects the absorption of waves in section 3. In section 4.1, the variance of wave absorption due to the variance of *D*-region electron densities measured by rockets is presented. Total wave absorption of waves under quiet, nonauroral *D*-region conditions is shown in section 4.2. We summarize our work and discuss possible extensions of current modeling of transionospheric VLF waves in section 5.

2. Calculation of Helliwell's Absorption Curves Using the Full Wave Method

[7] *Helliwell* [1965] calculated the total wave power absorption of VLF waves as $A_H = 8.69 \int \alpha dz$ in dB, with $\alpha \equiv \chi\omega/c$ and χ being the negative imaginary part of the R-mode wave refractive index, ω the angular wave frequency, and c the speed of light in vacuum. The R-mode wave refractive index is calculated using the quasi-longitudinal approximation in *Helliwell* [1965]. To eliminate errors due to reading data from figures of *Helliwell* [1965], we recalculate the total absorption of the R-mode wave as described by *Helliwell* [1965], except that we use the full whistler mode wave dispersion relation given by Appleton's equation (Equation (3.55) in *Helliwell* [1965]). The resulting total absorption A_H differs from the original absorption curves shown in Figure (3–35) of *Helliwell* [1965] (not shown here) by only few percentages, which is not enough to account for the difference between the modeling and observation shown by *Starks et al.* [2008].

[8] In order to isolate any potential effects introduced by our full wave code, we recalculate the absorption curves discussed above using our full wave code with the same ionospheric profile and a nontilted dipole magnetic field model with equatorial magnetic field strength $B_0 = 0.31$ G. We launch a linearly polarized plane wave vertically incident on the lower ionospheric boundary at $z = 60$ km and calculate the total absorption using $A_{HFW} = 10 \log_{10}[P(z = 1500 \text{ km})/P_{inc}]$. Here the wave power density $P \propto \mu(|E_x|^2 + |E_y|^2)$, with μ the real part of R-mode wave refractive index and the subscript "inc" denoting the incident wave at $z = 60$ km. Note that since we use a linearly polarized wave at $z = 60$ km, there is an extra 3 dB polarization loss present in A_{HFW} but not in A_H, as shown in Appendix B and *Helliwell* [1965], thus we reduce A_{HFW} by 3 dB when comparing to A_H.

[9] A comparison between $A_{HFW} - 3$ dB and A_H for 2 kHz and 20 kHz during daytime and nighttime is shown in Figure 2. Despite the different approaches, the total absorption calculated from the full wave code agrees very well with Helliwell's results. The small difference between the above two approaches is due to additional loss during the transition between layers as shown in Appendix B. The ripples in the absorption curve of the 2 kHz wave during nighttime, calculated by the full wave method, are due to the discontinuity in Helliwell's ionospheric density model: the lower ionosphere electron densities are independent of latitudes, while the upper ionosphere electron densities vary with latitude as described by *Helliwell* [1965]. This comparison shows that the full wave effect that has been omitted in Helliwell's approach is small, and Helliwell's absorption curves themselves are as accurate as the full wave results.

3. Wave Absorption from the IRI Model

[10] The simple ionospheric model of *Helliwell* [1965] does not reflect the temporal or spatial variation of the ionosphere, since it uses an ensemble averaged electron-density model. Some recent work on modeling transionospheric

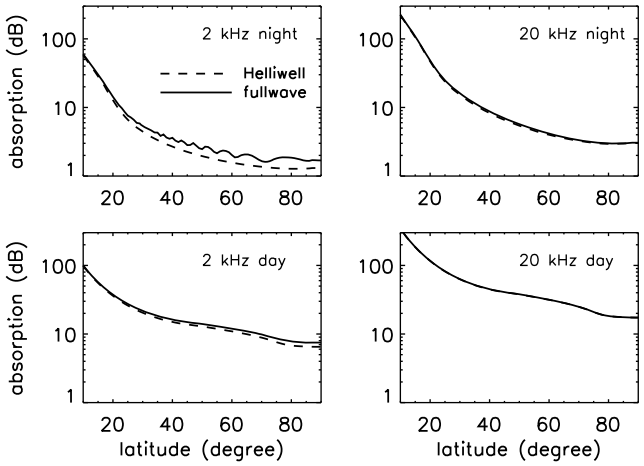

Figure 2. Comparison of the absorption of 2 kHz and 20 kHz waves using the approach of *Helliwell* [1965] (dashed lines) and the full wave method (solid lines). Note that a 3 dB polarization loss is removed from the full wave results.

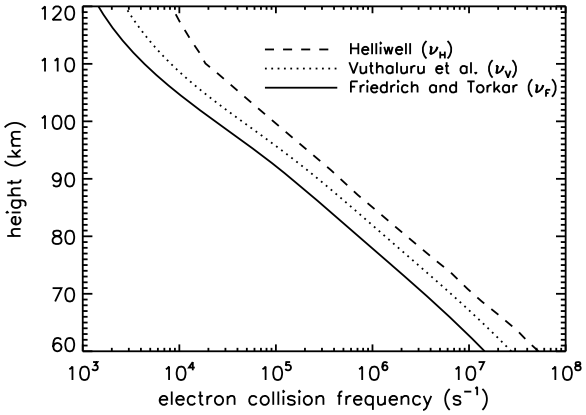

Figure 4. Comparison between electron collision frequencies in the *D* region of *Friedrich and Torkar* [1983] (solid line), *Vuthaluru et al.* [2002] (dotted line), and *Helliwell* [1965] (dashed line) at a representative latitude (10°). Collision frequency profiles ν_F and ν_V have weak latitudinal dependence.

propagation of waves uses the International Reference Ionosphere (IRI) model [*Lehtinen and Inan*, 2009; *Bilitza*, 2001; *Bilitza and Reinisch*, 2008]. In this section, we use the latest IRI model to provide electron density (N_{IRI}) in the ionosphere [*Bilitza and Reinisch*, 2008], calculate wave absorption with the full wave code and compare the results with Helliwell's absorption curves. The comparison between Helliwell's *D*-region electron-density profile (N_H) and N_{IRI} is shown in Figure 3. The IRI electron density is calculated for 15 December 1958, for comparison with *Helliwell* [1965]. Figure 3 shows that during daytime, N_H represents the mean density profile of the IRI model fairly well. The IRI densities at latitudes below 30° are generally higher than N_H while those at higher latitudes are lower. During nighttime, the IRI electron densities are generally lower than N_H, except at altitudes between about 80 km and 105 km.

[11] Since collisional absorption also depends on the collision frequency in the *D* region, we choose two collision frequency models of the *D* region (<120 km) in this section: *Friedrich and Torkar* [1983] (ν_F) and *Vuthaluru et al.* [2002] (ν_V). Both ν_F and ν_V are proportional to atmospheric pressure as $\nu_F = 6.41 \times 10^5\, p\ s^{-1}$ and $\nu_V = 1.21 \times 10^6\, p\ s^{-1}$, with p in Pa. The two collision frequency models are shown in Figure 4 together with the collision frequency profile used by Helliwell (ν_H) for comparison, which shows that $\nu_H \approx 2\nu_V \approx 4\nu_F$. The collision frequency profile above 120 km is calculated from *Banks* [1966] and the neutral atmosphere is modeled by NRLMSISE [*Picone et al.*, 2002].

[12] The combined effects of the different collision frequency and electron-density profiles on wave absorption are shown in Figure 5, where absorption of VLF waves using N_{IRI} with ν_V and ν_F is shown together with Helliwell's absorption (A_{HFW}) curves for reference. We see that ν_V gives overall

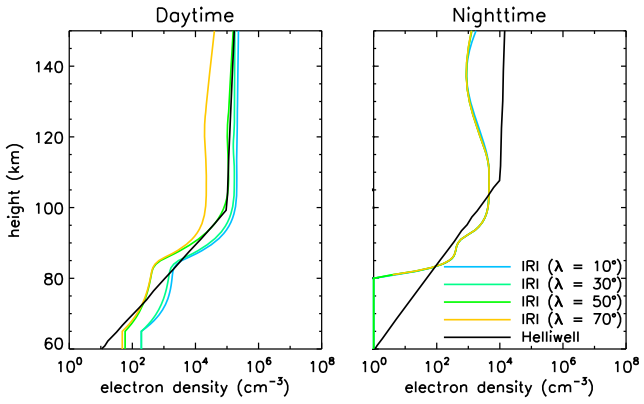

Figure 3. Comparison between electron densities in the *D* region of the model of *Helliwell* [1965] (black lines) and the IRI model at different latitudes (denoted by different colors).

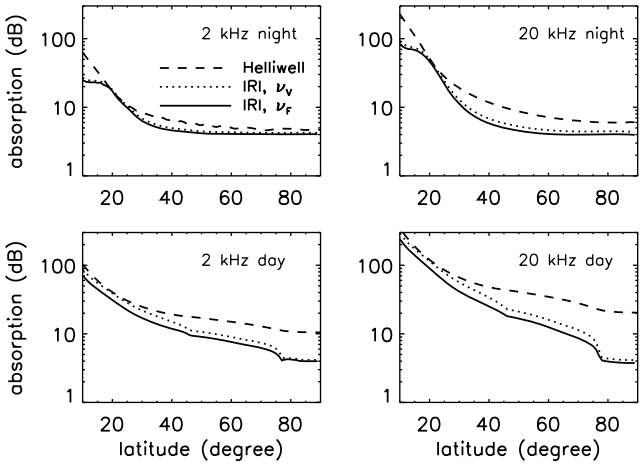

Figure 5. Comparison between the absorption of 2 kHz and 20 kHz waves using ionospheric models from IRI with ν_F (solid lines) or ν_V (dotted lines) and *Helliwell* [1965] (dashed lines).

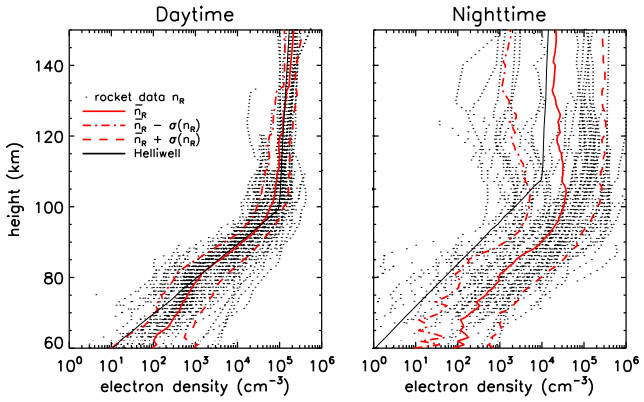

Figure 6. Comparison between electron densities measured by rockets (dots) and that of *Helliwell* [1965] (black lines). Also plotted are logarithmically mean electron density $\overline{n}_R$ (red solid lines) and its standard deviation $\overline{n}_R + \sigma(n_R)$ (red dashed lines) and $\overline{n}_R - \sigma(n_R)$ (red dash dotted lines).

only slightly higher wave absorption than ν_F, thus we will use only ν_F in the following analysis. During daytime, the total absorption of both 2 kHz and 20 kHz waves from IRI with ν_F is smaller than that from Helliwell by 5–10 dB for 2 kHz waves and 15–30 dB for 20 kHz waves. During nighttime, the IRI absorption curves agrees with Helliwell's curves for latitudes higher than 20° for 2 kHz waves, partly because the wave absorption of IRI and Helliwell are close to 3 dB at latitudes higher than 30°. The 3 dB loss is the polarization loss since the incident wave is a linearly polarized plane wave [*Helliwell*, 1965]. For 20 kHz waves, Helliwell's wave absorption is higher than that of IRI by 2–10 dB at latitudes higher than 25°. At latitudes less than 20°, wave absorption from the IRI model is lower than that of *Helliwell* [1965] by up to about 30 dB for 2 kHz waves and 100 dB for 20 kHz waves.

[13] Differences in wave absorption computed by this model mainly depend on the differences in electron collision frequency and density in the *D* region. Electron density in the *D*-region might vary by several orders of magnitude, and it might not be well modeled by the current IRI model [*Bilitza and Reinisch*, 2008]. In the next section, we use *D*-region electron densities measured by rockets during the last 60 years to show the expected variance of wave absorption.

4. Wave Absorption Calculated Using in Situ Measured D-Region Electron Densities

[14] *D*-region electron densities are principally obtained from in situ rocket measurements. In this section, we use electron-density profiles measured by rockets from 1947 to 2008 at various latitudes and local times. The same collection of data has been used to build the FIRI model [*Friedrich and Torkar*, 2001] for the nonauroral lower ionosphere and the IMAZ model for the auroral region [*McKinnell and Friedrich*, 2007]. We use data with local times between 10:00 and 14:00 as the local noon electron density and data between 22:00 and 02:00 as the local midnight electron density. We choose 4 h as the length of time window to provide enough data for a statistical analysis. We first show the statistical bounds of the variation of wave absorption using all measured *D*-region data. Then we show total wave absorption calculated using the *D*-region data under quiet, nonauroral conditions.

4.1. Statistical Bounds of Wave Absorption Variation Due to Change of D-Region Density

[15] The local noon and midnight electron densities from all rocket measured data (including the ones from high latitudes) are shown in Figure 6, together with Helliwell's *D*-region electron densities (N_H) for reference. The logarithmically averaged electron-density profiles $\overline{n}_R \equiv \exp[\sum_i \log(n_i)/N]$ together with standard deviation $\sigma(n_R)$ are shown as dashed lines. Here the summation is over the selected rocket measurements whose total number is N. The measurements indicate that the nighttime *D*-region electron density undergoes larger variation compared to the daytime, and its average value from 60 km to 100 km is generally higher than N_H by roughly an order of magnitude. The larger variance of nighttime *D*-region electron density is due to the large variability of the electron density in the auroral zone and is primarily related to the precipitation of electrons from the inner magnetosphere, which is a highly variable process. During daytime, however, N_H agrees with the mean measured density very well, except at altitudes below 80 km, where the mean measured density becomes gradually higher than N_H.

[16] To quantify the variance of the absorption curves due to variation in the *D*-region density, we use the mean electron density $\overline{n}_R$ and its standard deviation $\overline{n}_R \pm \sigma(n_R)$ to calculate wave absorption. The electron density above 150 km is obtained from the IRI model, and the collision frequency profile is the same as in section 3, shown in Figure 4. The absorption of 2 kHz and 20 kHz waves during daytime and nighttime is shown in Figure 7. The figure shows that Helliwell's absorption curves (A_{HFW}) generally lie within $A[\overline{n}_R \pm \sigma(n_R)]$ during both daytime and nighttime and is thus a good representation of the absorption in an averaged sense. However,

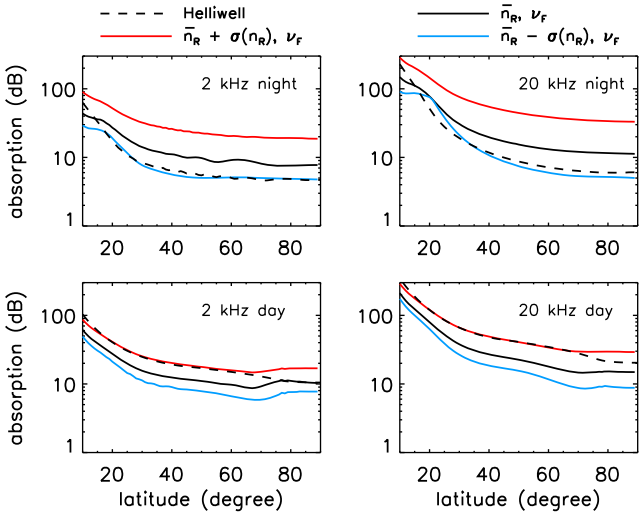

Figure 7. Comparison between the absorption curves of *Helliwell* [1965] (dashed lines) and wave absorptions calculated using $\overline{n}_R$ (black lines), $\overline{n}_R + \sigma(n_R)$ (red lines), and $\overline{n}_R - \sigma(n_R)$ (blue lines) with ν_F.

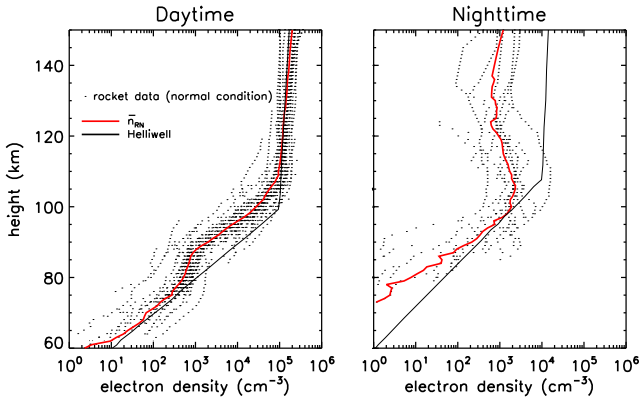

Figure 8. Comparison between electron densities measured by rockets under quiet, nonauroral conditions (dots), logarithmically mean electron densities $\overline{n}_{RN}$ (red lines), and that of *Helliwell* [1965] (black lines).

during nighttime, A_{HFW} is closer to $A[\overline{n}_R - \sigma(n_R)]$, and the mean absorption calculated using $\overline{n}_R$ is higher than A_{HFW} by about 3–10 dB for 2 kHz waves and about 5–15 dB for 20 kHz waves at latitudes higher than 20°. The wave absorption varies by about 15–60 dB for 2 kHz waves and 40–200 dB for 20 kHz waves due to the variance of electron densities in the *D* region. During daytime, A_{HFW} is closer to the absorption curves calculated from $\overline{n}_R + \sigma(n_R)$, and the mean absorption curves are lower than A_{HFW} by 10–30 dB because the collision frequency we use is smaller than that of Helliwell by about a factor of 4, as shown in Figure 4. The wave absorption varies by 10–40 dB for 2 kHz and 20–110 dB for 20 kHz waves due to the variance of electron densities in the *D* region. The smaller variance of wave absorption during daytime, compared with that of nighttime, is due to the smaller variance in the electron-density profile.

4.2. Wave Absorption Under Quiet, Nonauroral Conditions

[17] In the above calculation of statistical bounds on wave absorption, we used *D*-region rocket data under all conditions, which included quiet as well as disturbed periods and the data from the auroral zone. In this section, we calculate wave absorption under quiet conditions by excluding data containing effects of post storm, eclipse, winter anomaly, and auroral conditions. Also we only consider latitudes less than 60° to exclude the auroral zone or the polar cap. The average *D*-region electron-density profiles under quiet conditions ($\overline{n}_{RN}$) are shown in Figure 8. The daytime electron density is well represented by Helliwell's curve, except at altitudes between 80 and 110 km, where the average electron density $\overline{n}_{RN}$ is smaller than Helliwell's by about a factor of 10. The nighttime average electron density is generally smaller than Helliwell's by a factor up to 10.

[18] The total wave absorption calculated using average daytime and nighttime electron densities under quiet conditions is shown in Figure 9. As expected from the overall smaller electron density and collision frequency used, wave absorption from $\overline{n}_{RN}$ is smaller than A_{H}. During daytime, $A(\overline{n}_{RN})$ is smaller than A_{H} by 10–60 dB for 2 kHz and 25–100 dB for 20 kHz waves. During nighttime, the difference at latitudes above 20° is small, because of the overall small wave energy loss as discussed in section 3. For latitudes smaller than 20°, $A(\overline{n}_{RN})$ is smaller than A_{H} by up to about 35 dB for 2 kHz waves and 100 dB for 20 kHz waves.

5. Discussion and Summary

[19] In this paper, we verified Helliwell's calculation of wave absorption through the ionosphere using a full wave approach, implemented using the numerical method given by *Nagano et al.* [1975]. We showed that the full wave effects absent in *Helliwell* [1965] and errors caused by quasi-longitudinal approximation are negligible when using Helliwell's ionospheric model. We then used the IRI model and demonstrated that it gives overall smaller wave absorption compared with Helliwell's. The variance of wave absorption due to the variance of electron densities in the *D* region was then investigated using in situ electron-density data measured by rockets during the past 60 years. We showed that Helliwell's results are generally within ±1 standard deviation of the wave absorption calculated from rocket measured *D*-region electron-density data. However, the total absorption of waves shows large variance and is very sensitive to electron densities in the *D* region. Depending on local time and incident wave frequency, the total wave absorption might vary by 10–200 dB. Thus *D*-region electron-density variance should be taken into account when calculating collisional wave absorption by the ionosphere. The auroral *D*-region density, however, is typically larger than the *D*-region densities found near mid-latitude and low-latitude VLF transmitters. Thus we also calculated wave absorption using rocket data under quiet, nonauroral conditions. This wave absorption is smaller than that of Helliwell's by up to 100 dB for 20 kHz and 60 dB for 2 kHz. The result indicates that realistic *D*-region density would make the model-observation discrepancy shown by *Starks et al.* [2008] even larger. Additional processes are thus needed to explain the discrepancy. Interestingly, both IRI and rocket absorp-

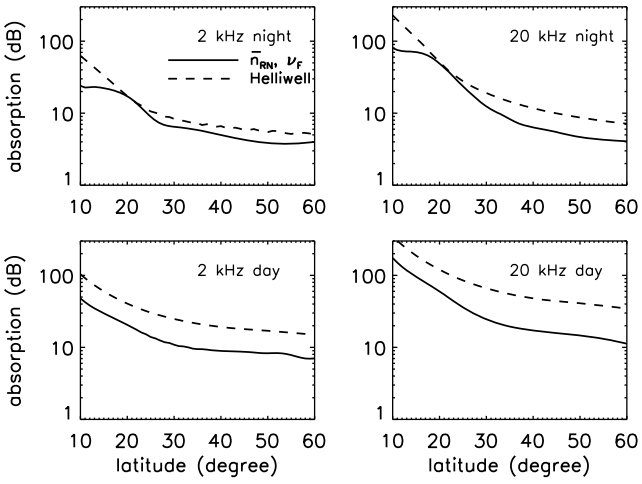

Figure 9. Comparison between the absorption curves of *Helliwell* [1965] (dashed lines) and wave absorption calculated using average *D*-region electron densities under quiet conditions $\overline{n}_{RN}$ and ν_{F} (black lines).

tion curves indicate that the equatorial absorption is lower than predicted by Helliwell's model by up to 100 dB and is consistent with observations showing a larger wave power than anticipated by models [*Starks et al.*, 2008]. Also our results suggest that Helliwell's absorption curves, while being accurate for the ionospheric model used, should not be applied in all situations, because variance in the *D*-region electron densities can cause large uncertainties in the results.

[20] In this study, we used rocket data to provide statistical bounds on wave absorption curves. We ignored the latitudinal dependence of the *D*-region electron density and used a vertically incident plane wave to make a direct comparison with *Helliwell* [1965]. In order to make a more realistic model-observation comparison like *Starks et al.* [2008], we should use a realistic wave radiation pattern of ground based transmitters, combined with a suitable *D*-region electron-density model [e.g., *Friedrich and Torkar*, 2001]. This study will be the subject of future work.

Appendix A: Generalized Full Wave Equations

[21] The ionosphere is assumed to be a stratified medium as shown in Figure 1. The *x*-*y* plane is parallel to boundaries of layers, and the *z* axis is along the normal direction to the boundaries. *Nagano et al.* [1975] considered a coordinate system where the $\boldsymbol{k}$ vector is in the *x*-*z* plane, and the magnetic field $\boldsymbol{B}$ vector has arbitrary direction cosines ($l_{\boldsymbol{B}}$, $m_{\boldsymbol{B}}$, $n_{\boldsymbol{B}}$). In this section, we generalize the work of *Nagano et al.* [1975], so that $\boldsymbol{k}$ can also have arbitrary direction cosines ($l_{\boldsymbol{k}}$, $m_{\boldsymbol{k}}$, $n_{\boldsymbol{k}}$). This is useful when we want to calculate, e.g., a spheric wave propagating through the ionosphere. We also include ions in the calculation, even though their contribution to wave absorption is negligible in the VLF frequency range.

[22] Assuming that the wavefields vary with time as $e^{j\omega t}$, where $j \equiv \sqrt{-1}$, we have Maxwell's equations

$$\nabla \times \boldsymbol{H} = j\omega\epsilon_0(\mathsf{I} + \mathsf{M}) \cdot \boldsymbol{E}, \tag{A1}$$

$$\nabla \times \boldsymbol{E} = -j\omega\mu_0 \boldsymbol{H}, \tag{A2}$$

where ϵ_0, μ_0, and I are the permittivity, the permeability of free space, and the unit matrix, respectively. The susceptibility matrix M can be obtained from the Lorentz equations of motion, and it is given by

$$\mathsf{M} = \begin{bmatrix} M_{xx} & M_{xy} & M_{xz} \\ M_{yx} & M_{yy} & M_{yz} \\ M_{zx} & M_{zy} & M_{zz} \end{bmatrix},$$

with

$$\begin{aligned}
M_{xx} &= l_{\boldsymbol{B}}^2 P + (1 - l_{\boldsymbol{B}}^2)S - 1, \\
M_{xy} &= m_{\boldsymbol{B}} l_{\boldsymbol{B}}(P - S) + j n_{\boldsymbol{B}} D, \\
M_{xz} &= n_{\boldsymbol{B}} l_{\boldsymbol{B}}(P - S) - j m_{\boldsymbol{B}} D, \\
M_{yx} &= m_{\boldsymbol{B}} l_{\boldsymbol{B}}(P - S) - j n_{\boldsymbol{B}} D, \\
M_{yy} &= m_{\boldsymbol{B}}^2 P + (1 - m_{\boldsymbol{B}}^2)S - 1, \\
M_{yz} &= m_{\boldsymbol{B}} n_{\boldsymbol{B}}(P - S) + j l_{\boldsymbol{B}} D, \\
M_{zx} &= n_{\boldsymbol{B}} l_{\boldsymbol{B}}(P - S) + j m_{\boldsymbol{B}} D, \\
M_{zy} &= m_{\boldsymbol{B}} n_{\boldsymbol{B}}(P - S) - j l_{\boldsymbol{B}} D, \\
M_{zz} &= n_{\boldsymbol{B}}^2 P + (1 - n_{\boldsymbol{B}}^2)S - 1,
\end{aligned}$$

where we have included effects of ions through the use of Stix parameters *P*, *S*, and *D* with collisions between particles considered [*Stix*, 1962]. They are defined as $P = 1 - \sum_i \omega_{pi}^2/\omega^2$, $S = (R + L)/2$, and $D = (R - L)/2$, where $R = 1 - \sum_i \omega_{pi}^2/[\omega/(\omega + \Omega_i)]$ and $L = 1 - \sum_i \omega_{pi}^2/[\omega(\omega - \Omega_i)]$. Here the modified plasma frequency ω_{pi} and gyrofrequency Ω_i of the i_{th} species due to collision are

$$\begin{aligned}
\omega_{pi}^2 &= \frac{q_i^2 N_i}{\epsilon_0 m_i (1 - j\nu_i/\omega)}, \\
\Omega_i &= \frac{q_i B}{m_i (1 - j\nu_i/\omega)},
\end{aligned}$$

with N_i the number density, q_i the charge, m_i the mass and ν_i the collision frequency of the i_{th} species. All units are in MKS.

[23] Assuming that the wavefields vary as $e^{-jk(l_{\boldsymbol{k}}x + m_{\boldsymbol{k}}y)}$ in the *x* and *y* direction, with Snell's law, it can be demonstrated that the *x* and *y* components of electric and magnetic fields satisfy

$$\frac{d\boldsymbol{e}}{dz} = -jk\mathsf{T} \cdot \boldsymbol{e}, \tag{A3}$$

with $k \equiv \omega/c$ the wave normal vector in vacuum and $\boldsymbol{e}$ is defined by

$$\boldsymbol{e} = \begin{vmatrix} E_x \\ -E_y \\ Z_0 H_x \\ Z_0 H_y \end{vmatrix}, \tag{A4}$$

with $Z_0 = \sqrt{\mu_0/\epsilon_0}$. Here T is given by

$$\mathsf{T} = \begin{bmatrix}
\dfrac{-l_{\boldsymbol{k}} M_{zx}}{1 + M_{zz}} & \dfrac{l_{\boldsymbol{k}} M_{zy}}{1 + M_{zz}} & \dfrac{l_{\boldsymbol{k}} m_{\boldsymbol{k}}}{1 + M_{zz}} & 1 - \dfrac{l_{\boldsymbol{k}}^2}{1 + M_{zz}} \\
\dfrac{m_{\boldsymbol{k}} M_{zx}}{1 + M_{zz}} & \dfrac{-m_{\boldsymbol{k}} M_{zy}}{1 + M_{zz}} & 1 - \dfrac{m_{\boldsymbol{k}}^2}{1 + M_{zz}} & \dfrac{m_{\boldsymbol{k}} l_{\boldsymbol{k}}}{1 + M_{zz}} \\
-M_{yx} - m_{\boldsymbol{k}} l_{\boldsymbol{k}} + \dfrac{M_{yz} M_{zx}}{1 + M_{zz}} & 1 + M_{yy} - l_{\boldsymbol{k}}^2 - \dfrac{M_{yz} M_{zy}}{1 + M_{zz}} & \dfrac{-m_{\boldsymbol{k}} M_{yz}}{1 + M_{zz}} & \dfrac{M_{yz} l_{\boldsymbol{k}}}{1 + M_{zz}} \\
1 + M_{xx} - m_{\boldsymbol{k}}^2 - \dfrac{M_{xz} M_{zx}}{1 + M_{zz}} & -M_{xy} - l_{\boldsymbol{k}} m_{\boldsymbol{k}} + \dfrac{M_{xz} M_{zy}}{1 + M_{zz}} & \dfrac{m_{\boldsymbol{k}} M_{xz}}{1 + M_{zz}} & \dfrac{-l_{\boldsymbol{k}} M_{xz}}{1 + M_{zz}}
\end{bmatrix}.$$

Equation (A3) is then solved using the matrix method described by *Nagano et al.* [1975].

Appendix B: Difference Between Helliwell's Approach and a Full Wave Method

[24] With a stratified ionospheric model, the total energy loss through ionosphere in the full wave code can be written as

$$A_{\mathrm{HFW}} \equiv -10\log_{10}\frac{P_{\mathrm{R}}\left(z_{m-1}^{+}\right)}{P_{\mathrm{inc}}\left(z_{0}^{-}\right)} = -10\left[\log_{10}\frac{P_{\mathrm{R}}\left(z_{m-1}^{+}\right)}{P_{\mathrm{R}}\left(z_{m-2}^{+}\right)} + \log_{10}\frac{P_{\mathrm{R}}\left(z_{m-2}^{+}\right)}{P_{\mathrm{R}}\left(z_{m-3}^{+}\right)} + \cdots + \log_{10}\frac{P_{\mathrm{R}}\left(z_{1}^{+}\right)}{P_{\mathrm{R}}\left(z_{0}^{+}\right)} + \log_{10}\frac{P_{\mathrm{R}}\left(z_{0}^{+}\right)}{P_{\mathrm{inc}}\left(z_{0}^{-}\right)}\right], \tag{B1}$$

where z_k^+ means the location just above the boundary z_k and z_k^- means the location just below it. We differentiate between $P_{\mathrm{R}}(z_k^-)$ and $P_{\mathrm{R}}(z_k^+)$ because this gives the difference in total absorption between a full wave calculation and *Helliwell* [1965] calculation, if any. We have replaced $P(z_{m-1})$ in the equation of A_{HFW} by $P_{\mathrm{R}}(z_{m-1}^+)$, because the R-mode wave is the only wave mode that can penetrate through the ionosphere in this frequency range; the L-mode wave is simply damped away. Note that the last term on the right-hand side of the above equation has been pointed out by *Helliwell* [1965] as the polarization loss with a value of 3 dB in the case that the incident wave is linearly polarized. On the other hand, the calculation done by *Helliwell* [1965] can be regarded as

$$A_{\mathrm{H}} \approx 8.69\sum_{i=0}^{m-2}\alpha_i(z_{i+1}-z_i) = -10\left[\log_{10}\frac{P_{\mathrm{R}}\left(z_{1}^{-}\right)}{P_{\mathrm{R}}\left(z_{0}^{+}\right)} + \cdots + \log_{10}\frac{P_{\mathrm{R}}\left(z_{m-2}^{-}\right)}{P_{\mathrm{R}}\left(z_{m-3}^{+}\right)} + \log_{10}\frac{P_{\mathrm{R}}\left(z_{m-1}^{-}\right)}{P_{\mathrm{R}}\left(z_{m-2}^{+}\right)}\right]. \tag{B2}$$

The difference between A_{HFW} and A_{H} is

$$A_{\mathrm{HFW}} - A_{\mathrm{H}} = -10\left[\log_{10}\frac{P_{\mathrm{R}}\left(z_{m-1}^{+}\right)}{P_{\mathrm{R}}\left(z_{m-1}^{-}\right)} + \log_{10}\frac{P_{\mathrm{R}}\left(z_{m-2}^{+}\right)}{P_{\mathrm{R}}\left(z_{m-2}^{-}\right)} + \cdots + \log_{10}\frac{P_{\mathrm{R}}\left(z_{0}^{+}\right)}{P_{\mathrm{inc}}\left(z_{0}^{-}\right)}\right]. \tag{B3}$$

[25] It has been shown in Figure 2 that the above difference between A_{HFW} and A_{H}, shown in equation (B3), is less than 1 dB, besides the polarization loss. Thus the full wave effects absent in Helliwell's approach are negligible.

[26] **Acknowledgments.** Xin Tao and Jacob Bortnik thank Richard Thorne and Jay Albert for helpful discussions and the U.S. Office of Naval Research award number N00014-08-1-1232 for supporting this project.

[27] Robert Lysak thanks Michael Starks and another reviewer for their assistance with this paper.

References

Abel, B., and R. M. Thorne (1998a), Electron scattering loss in Earth's inner magnetosphere, 1. Dominant physical processes, *J. Geophys. Res.*, *103*(A2), 2385–2396.

Abel, B., and R. M. Thorne (1998b), Electron scattering loss in Earth's inner magnetosphere, 2. Sensitivity to model parameters, *J. Geophys. Res.*, *103*(A2), 2397–2407.

Arantes, D. S., and R. R. Scarabucci (1975), Full-wave analysis and coupling effects in a crossover region, *Radio Sci.*, *10*(8,9), 801–811.

Banks, P. (1966), Collision frequencies and energy transfer electrons, *Planet. Space Sci.*, *14*, 1085–1103.

Bilitza, D. (2001), International reference ionosphere 2000, *Radio Sci.*, *36*(2), 261–275.

Bilitza, D., and B. Reinisch (2008), International reference ionosphere 2007: Improvements and new parameters, *Adv. Space Res.*, *42*, 599–609.

Bortnik, J., U. S. Inan, and T. F. Bell (2006a), Temporal signatures of radiation belt electron precipitation induced by lightning-generated MR whistler waves, 1. Methodology, *J. Geophys. Res.*, *111*, A02204, doi:10.1029/2005JA011182.

Bortnik, J., U. S. Inan, and T. F. Bell (2006b), Temporal signatures of radiation belt electron precipitation induced by lightning-generated MR whistler waves, 2. Global signatures, *J. Geophys. Res.*, *111*, A02205, doi:10.1029/2005JA011398.

Budden, K. G. (1985), *The Propagation of Radio Waves: The Theory of Radio Waves of Low Power in the Ionosphere and Magnetosphere*, Cambridge University Press, Cambridge, U. K.

Friedrich, M., and K. M. Torkar (1983), Collision frequencies in the high-latitude *D*-region, *J. Atmos. Sol. Terr. Phys.*, *45*(4), 267–271.

Friedrich, M., and K. M. Torkar (2001), FIRI: A semiempirical model of the lower ionosphere, *J. Geophys. Res.*, *106*(A10), 21,409–21,418.

Helliwell, R. A. (1965), *Whistlers and Related Ionospheric Phenomena*, Stanford University Press, Stanford, California.

Inan, U. S., H. C. Chang, and R. A. Helliwell (1984), Electron precipitation zones around major ground-based VLF signal sources, *J. Geophys. Res.*, *89*(A5), 2891–2906.

Lehtinen, N. G., and U. S. Inan (2008), Radiation of ELF/VLF waves by harmonically varying currents into a stratified ionosphere with application to radiation by a modulated electrojet, *J. Geophys. Res.*, *113*, A06301, doi:10.1029/2007JA012911.

Lehtinen, N. G., and U. S. Inan (2009), Full-wave modeling of transionospheric propagation of VLF waves, *Geophys. Res. Lett.*, *36*, L03104, doi:10.1029/2008GL036535.

McKinnell, L.-A., and M. Friedrich (2007), A neural network-based ionospheric model for the auroral zone, *J. Atmos. Sol. Terr. Phys.*, *69*, 1459–1470, doi:10.1016/j.jastp.2007.05.003.

Nagano, I., M. Mambo, and G. Hutatsuishi (1975), Numerical calculation of electromagnetic waves in an anisotropic multilayered medium, *Radio Sci.*, *10*(6), 611–617.

Picone, J. M., A. E. Hedin, D. P. Drob, and A. C. Aikin (2002), NRLMSISE-00 empirical model of the atmosphere: Statistical comparisons and scientific issues, *J. Geophys. Res.*, *107*(A12), 1468, doi:10.1029/2002JA009430.

Pitteway, M. L. V. (1965), The numerical calculation of wave-fields, reflection coefficient and polarizations for long radio waves in the lower ionosphere, I. *Phil. Trans. R. Soc. London*, *257*, 219–241.

Schunk, R. W., and A. F. Nagy (2004), *Ionospheres: Physics, Plasma Physics, and Chemistry*, Cambridge University Press, Cambridge, U. K.

Starks, M. J., R. A. Quinn, G. P. Ginet, J. M. Albert, G. S. Sales, B. W. Reinisch, and P. Song (2008), Illumination of the plasmasphere by terrestrial very low frequency transmitters: Model validation, *J. Geophys. Res.*, *113*, A09320, doi:10.1029/2008JA013112.

Stix, T. H. (1962), *The Theory of Plasma Waves*, McGraw-Hill, New York.

Vuthaluru, R., R. A. Vincent, D. A. Holdsworth, and I. M. Reid (2002), Collision frequencies in the *D*-region, *J. Atmos. Sol. Terr. Phys.*, *64*, 2043–2054, doi:10.1016/S1364-6826(02)00220-1.

Walsh, E. J. (1967), Full-wave solutions in terms of coupled vacuum modes, *Radio Sci.*, *2*(8), 913.

J. Bortnik and X. Tao, Department of Atmospheric and Oceanic Sciences, University of California, Los Angeles, 100 Stein Plaza Driveway, Los Angeles, CA 90095-7065, USA. (xtao@atmos.ucla.edu)

M. Friedrich, Institute of Communication Networks and Satellite Communications, Graz University of Technology, Inffeldgasse 12, A-8010 Graz, Austria.